Neuro-Oncology
19(1), 109–117, 2017 | doi:10.1093/neuonc/now121 | Advance Access date 26 June 2016

Multimodal MRI features predict isocitrate dehydrogenase genotype in high-grade gliomas

Biqi Zhang, Ken Chang, Shakti Ramkissoon, Shyam Tanguturi, Wenya Linda Bi, David A. Reardon, Keith L. Ligon, Brian M. Alexander, Patrick Y. Wen, and Raymond Y. Huang

Department of Radiology, Brigham and Women's Hospital, Boston, Massachusetts (B.Z., K.C., R.Y.H.); Department of Pathology, Brigham and Women's Hospital, Boston, Massachusetts (S.R., K.L.L.); Department of Pathology, Harvard Medical School, Boston, Massachusetts (S.R., K.L.L.); Department of Pathology, Boston Children's Hospital, Boston, Massachusetts (S.R., K.L.L.); Department of Medical Oncology, Dana-Farber Cancer Institute, Boston, Massachusetts(S.R., D.A.R., K.L.L., P.Y.W.); Harvard Radiation Oncology Program, Boston, Massachusetts (S.T.); Department of Neurosurgery, Brigham and Women's Hospital, Boston, Massachusetts (W.L.B.); Center of Neuro-Oncology, Dana-Farber/Brigham and Women's Cancer Center, Boston, Massachusetts (D.A.R., P.Y.W.); Department of Radiation Oncology, Dana-Farber/Brigham and Women's Cancer Center, Boston, Massachusetts (B.M.A.)

Corresponding author: Raymond Huang, MD, PhD, Department of Radiology, Brigham and Women's Hospital, 75 Francis Street, Boston, MA 02445 (ryhuang@partners.org).

Abstract

Background. High-grade gliomas with mutations in the isocitrate dehydrogenase (*IDH*) gene family confer longer overall survival relative to their *IDH*-wild-type counterparts. Accurate determination of the *IDH* genotype preoperatively may have both prognostic and diagnostic value. The current study used a machine-learning algorithm to generate a model predictive of *IDH* genotype in high-grade gliomas based on clinical variables and multimodal features extracted from conventional MRI.

Methods. Preoperative MRIs were obtained for 120 patients with primary grades III ($n = 35$) and IV ($n = 85$) glioma in this retrospective study. *IDH* genotype was confirmed for grade III (32/35, 91%) and IV (22/85, 26%) tumors by immunohistochemistry, spectrometry-based mutation genotyping (OncoMap), or multiplex exome sequencing (OncoPanel). *IDH1* and *IDH2* mutations were mutually exclusive, and all mutated tumors were collapsed into one *IDH*-mutated cohort. Cases were randomly assigned to either the training ($n = 90$) or validation cohort ($n = 30$). A total of 2970 imaging features were extracted from pre- and postcontrast T1-weighted, T2-weighted, and apparent diffusion coefficient map. Using a random forest algorithm, nonredundant features were integrated with clinical data to generate a model predictive of *IDH* genotype.

Results. Our model achieved accuracies of 86% (area under the curve [AUC] = 0.8830) in the training cohort and 89% (AUC = 0.9231) in the validation cohort. Features with the highest predictive value included patient age as well as parametric intensity, texture, and shape features.

Conclusion. Using a machine-learning algorithm, we achieved accurate prediction of *IDH* genotype in high-grade gliomas with preoperative clinical and MRI features.

Key words

high-grade glioma | isocitrate dehydrogenase | machine learning | MRI | prediction

High-grade gliomas constitute the most common primary adult brain malignancy, with an incidence of 3.68 per 100 000.[1] Prognosis is grim despite the best available therapies. Five-year survival rates are 27.3% to 52.2% for WHO grade III gliomas, depending on the subtype, and only 5% for WHO grade IV gliomas.[1] Recent genomic characterization of these tumors has shown, however, that mutations in the isocitrate dehydrogenase 1 (*IDH1*) gene, or its homolog *IDH2*, are associated with longer overall survival in high-grade gliomas relative to their wild-type

(WT) counterparts and independent of histologic grade.[2–5] Grade IV gliomas that have acquired *IDH1* or *IDH2* (*IDH*) mutations have a median overall survival of 31 months as compared with 15 months for those with WT *IDH*.[2] Among high-grade gliomas, patients with *IDH*-WT grade III tumors also exhibit worse prognosis than those with *IDH*-mutated grade IV tumors.[6]

The *IDH* gene product normally converts isocitrate into α-ketoglutarate, while mutations in the *IDH* gene family result in enzyme products that instead drive conversion of isocitrate into 2-hydroxyglutarate (2-HG). 2-HG competitively inhibits downstream histone demethylases, which contributes to abnormal regulation of gene expression in these cancers.[7]

At present, the most commonly used method for assessing *IDH* mutation status is immunohistochemical analysis following biopsy or surgical resection. Multiple exome sequencing studies have demonstrated, however, that up to 15% of *IDH*-mutated gliomas are not detected by traditional IDH1 (p.R132H) antibody testing.[8,9] In addition, while biopsy for most intracranial masses can be performed with relatively low risk, a noninvasive method for preoperative prediction may be helpful for operative planning; a recent study suggested that subtotal resection of enhancing tumor was associated with longer overall survival in *IDH*-WT high-grade glioma, whereas only complete resection including both enhancing and nonenhancing components of tumor improved survival in *IDH*-mutated gliomas.[10] It is these aspects of *IDH*-WT and *IDH*-mutated high-grade glioma that increase the impetus for preoperative determination of *IDH* genotype with methods such as MRI.

Genomic alterations in gliomas are associated with a number of radiographic features on MRI.[11] Several of these standard imaging features including unilateral growth, tumor margin sharpness, and signal intensity heterogeneity vary significantly with *IDH* genotype and prognosis, although these associations have largely been based on univariate analyses.[12,13] Single imaging features are expected to perform less well in predicting *IDH* genotype in HHGs as a result of greater tumor heterogeneity.[14,15] Studies correlating the genetic and clinical features of glioma based on qualitative imaging analysis such as degree of enhancement and appearance of tumor margins are prone to interrater variability.[16]

In recent years, machine-learning algorithms have been applied to imaging studies of gliomas to predict genotype and patient survival outcomes based on imaging features extracted from conventional MRI.[17–20] In this study, we retrospectively examined the preoperative MRI of 120 patients diagnosed with either primary grade III or IV glioma with known *IDH* genotype. We hypothesized that a model integrating multimodal MRI features using a machine-learning approach could accurately predict *IDH* genotype in HGGs.

Methods

Patient Enrollment

This study was conducted following approval by the Dana-Farber/Brigham and Women's Cancer Center (DF/BWCC) Institutional Review Board (IRB). MR imaging, clinical variables including primary patient demographics (ie, age, sex, KPS, and preoperative steroid use), and genotyping data were obtained from the medical record under a consented research protocol approved by the DF/BWCC IRB (11-104). We retrospectively identified patients who met the following criteria: (i) histopathologically confirmed primary grade III or IV glioma according to current WHO criteria,[21] (ii) known *IDH* genotype, and (iii) available preoperative MRI consisting of precontrast axial T1-weighted (T1), postcontrast axial T1-weighted (T1c), axial T2-weighted fast spin echo (FSE, T2), T2-weighted fluid attenuation inversion recovery (T2/FLAIR) images, and MR-diffusion weighted imaging (DWI). Patients with secondary HGGs were excluded from this study. Patients whose genetic data were not confirmed per criteria (see "Tissue Diagnosis and Genotyping" section below) and whose tumors did not demonstrate contrast enhancement were excluded. Our final cohort included 120 patients with primary grade III ($n = 35$) and grade IV ($n = 85$) gliomas.

Tissue Diagnosis and Genotyping

All sequencing assays were performed within the Molecular Diagnostics Division of the Brigham and Women's Hospital Center for Advanced Molecular Diagnostics, a CLIA-certified laboratory environment. *IDH1/2* mutations were determined using immunohistochemistry,[22] mass spectrometry-based mutation genotyping (OncoMap),[22,23] or multiplex exome sequencing (OncoPanel)[8,24] depending on which genotyping technologies were available at the time of diagnosis. For this retrospective study, only gliomas with absence of *IDH1/2* mutations as determined by full sequencing assay with OncoPanel, were included in our analyses as *IDH*-WT gliomas. *IDH*-mutated gliomas were defined by the presence of mutation as indicated by immunohistochemistry or either of the 2 sequencing methods.

Briefly, diaminobenzidine (DAB) brightfield staining was performed according to standard protocols on 5-micron thick paraffin sections. Antigens were retrieved using heat and 10 mM sodium citrate buffer (pH 6.0), and the following primary antibody was utilized: IDH1(R132H) (Dianova, DIA-H05). Counterstaining for nuclei was performed using Mayer's hematoxylin stain, and coverslips were mounted with Permount (Fisher Scientific). OncoMap is a multiplexed Sequenom-based assay to detect somatic mutations in tumor DNA and was performed in the DF/BWCC CLIA-certified laboratory. OncoMap v4 detects mutations in 471 different loci from 41 cancer genes. OncoPanel (Illumina HiSeq) is a DNA-based next-generation sequencing assay that detects somatic mutations in 275 different cancer genes including *IDH1* and *IDH2*.

MRI Data Acquisition and Preprocessing

Standard MR imaging protocol for brain tumors at our institution includes nonenhanced sagittal and axial T1-weighted imaging, axial T2-weighted FSE and T2/FLAIR imaging, contrast-enhanced axial T1-weighted imaging, and 3D spoiled gradient echo (SPGR) imaging with coronal and sagittal reconstructions. Gadopentetate dimeglumine

(Magnevist, Bayer Healthcare) was administered for contrast-enhanced imaging.

MR-DWI images were acquired before injection of contrast and were obtained with TE/TR 80–110 ms/4–10 s, section thickness 5 mm with 1 mm intersection gap, matrix size 128 × 128, and FOV 22–25 cm by using monopolar spin-echo echo-planar preparation. Apparent diffusion coefficient (ADC) images were calculated from acquired DWI with b-values of 0 s/mm^2 and 1000 s/mm^2 images. ADC maps were generated using Advantage Workstation (version 4.3, GE Healthcare). All MR images were transferred to a high-performance cluster server for post processing.[25]

Volumetric Tumor Segmentation

Figure 1 provides an overview of our MRI processing pipeline. The computer-based Brain Tumor Image Analysis (BraTumIA, version 1.2) software was used to co-register and skull-strip T1, T1c, T2, and T2/FLAIR images. The segmentation protocol was completed as described previously.[26] Briefly, whole tumor volume, which includes solid tumor, infiltrating tumor, and edema, were segmented from FLAIR imaging. The T1c images from MRI were used for enhancing-tumor volume segmentation. Enhancing-tumor volume was subtracted from whole tumor volume to obtain the nonenhancing tumor volume. 3D Slicer Software (version 4.1), a user-driven manual active contour segmentation tool, was used to segment tumor volumes.[27,28] The segmented volume contour was overlaid with source T1c and T2/FLAIR images and edited by the study neuroradiologist (R.Y.H.) to manually add pixels for tumor regions not included in the preliminary contour or remove pixels for nontumor regions included in the preliminary contour.

Generation of Subregional Volume Mask

Additional volumes were calculated within whole tumor, enhanced tumor, and nonenhanced tumor volume segmentations. Regions with ADC values <1100 and 1350 × 10^{-6} mm^2/s were segmented. In addition, to characterize tumor margins, edge submasks were calculated by detecting the edge of whole tumor and enhanced tumor volumes, then width dilations to lengths of 5 voxels outside and 3 voxels inside this edge. The resulting edge submasks have an 8 voxel width that captures regions of both tumor and normal-appearing brain.

MRI Feature Extraction

For each glioma case, we extracted 5 categories of features (anatomical location, shape, texture, multimodal voxel parametric, and histogram) from volume masks and submasks to maximize the characterization of the tumor.

Anatomical features were defined by the study radiologist (R.Y.H.) by region (frontal, temporal, parietal, occipital, and deep brain) and laterality (left, right). The remaining shape, texture, multimodal parametric features, and ADC features were calculated from MRI (Supplemental Materials Section).

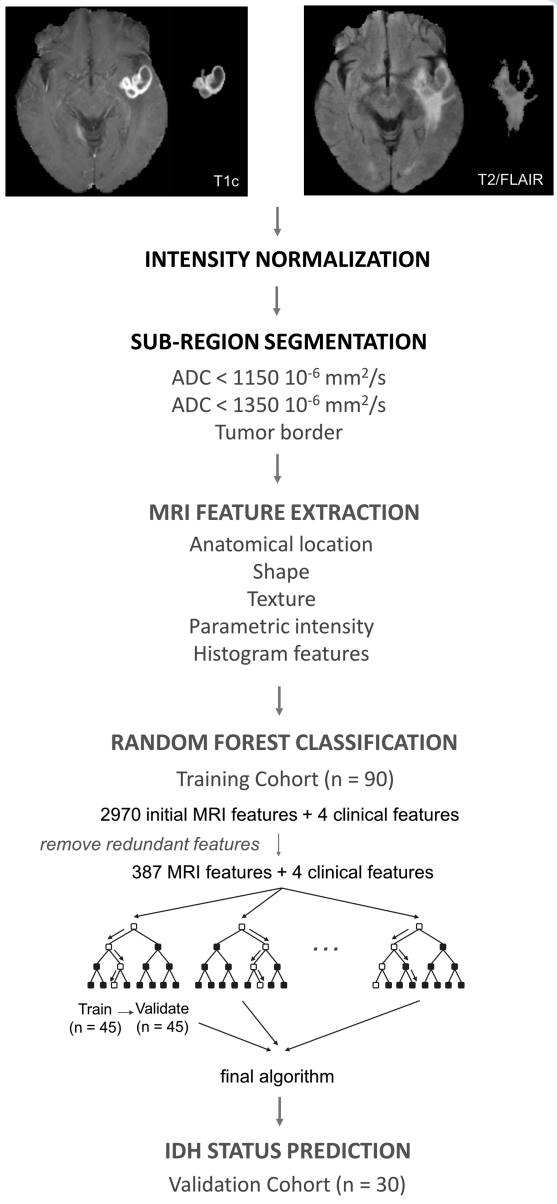

Fig. 1 MRI feature extraction and machine-learning pipeline.

Classification Procedure

The machine-learning procedure was performed using the Statistics and Machine Learning Toolbox MATLAB 2015a. We applied the random forest algorithm to generate a model predictive of *IDH* genotype. Random forest is one of several machine-learning algorithms that have been applied in clinical classification problems. It is especially advantageous when the number of predictor variables greatly exceeds sample size because it is resistant to overfitting.[29] This method has been applied successfully for identifying single-nucleotide polymorphisms among millions of mutations in known DNA repair pathways that may contribute to the development of grade IV glioma.[30] This

approach can also distinguish low-grade from high-grade gliomas by MRI features from area under the receiver operating characteristic (AUROC) analysis.[31]

Building a classifier involved growing multiple decision trees based on random selection of predictors (ie, MRI features) and random selection of data (ie, glioma cases). In this study, all 120 patients were randomly assigned to either the training cohort (n = 90) or validation cohort (n = 30). All cases in the training cohort were used to train the classifier, while cases in the validation cohort were used to independently evaluate the performance of the final model.

In implementing the random forest algorithm, we specified 3 parameters: (i) the number of features used during the training process, (ii) the maximum depth of the trees, and (iii) the number of trees grown. The predictive value of each MRI feature for determining *IDH* genotype was calculated individually by AUROC analysis. Features with AUC values >0.7 were then isolated and ranked. Redundant features, which were defined as features with a Spearman rank correlation coefficient >0.7, $P < .05$ with another feature of higher AUC, were removed. The remaining 386 features were used in our training algorithm. The tree depth was set to 64, and the algorithm was set to grow to a total of 4096 trees, a number empirically determined to be a reasonable upper bound in our learning models and before which the training set classification error commonly begins to converge.[32]

Individual trees were grown by taking a bootstrap sample from the training cohort with a fixed boot fraction of one-half. For each tree, growth at each branch utilized all 386 MRI features, and bootstrapped cases were used to grow the tree while the remaining out-of-bag cases were used as the test set. The random forest algorithm integrated all decorrelated trees to create a final classifier. Ten-fold cross validation was also applied to calculate misclassification error of our model within the training cohort. Finally, the model was tested on the validation cohort using the same model score threshold selected based on AUROC analysis of the training set. Subgroup analyses were also performed to test the final model on grade III and grade IV gliomas individually.

Features with most significant contributions to the final model were determined by the increase in prediction error if the values of that feature were permuted across the out-of-bag observations. This measure was computed for every tree and then averaged over the entire ensemble and divided by the standard deviation over the entire ensemble.[33]

Statistical Analysis

All statistical analyses were performed using the Statistics and Machine Learning Toolbox 2015a (MATLAB). For comparison of mean model score between *IDH*-WT and -mutated high-grade gliomas, the Student t test was used with significance defined as <0.05.

Results

Patient Characteristics

MRI images were obtained from 120 patients with primary grade III (n = 35, 17 male [49%], age range 23y–72y) and grade IV (n = 85, 35 male [41%], age range 21y–85y) gliomas. *IDH* mutations were identified in 32 of 35 (91%) grade III gliomas and in 22 of 85 (26%) grade IV gliomas. One grade IV tumor harbored an *IDH2* mutation; all other *IDH*-mutated tumors had *IDH1* mutations. The proportion of *IDH*-mutated tumors in our grade IV cohort was higher than usual due to exclusion of *IDH*-WT gliomas that did not have sequencing data to confirm genotype. *IDH1* and *IDH2* mutations were mutually exclusive in our cohort, consistent with previous reports.[34,35] As such, *IDH1*- and *IDH2*-mutated gliomas were collapsed into one category. Each glioma was then randomly assigned to either the training or validation cohort in the learning model (Table 1).

Because of the retrospective nature of this study, KPS at the time of imaging was unfortunately unavailable for our cohort. Data on steroid use at the time of imaging were available for 91 patients (53 *IDH*-WT, 38 *IDH*-mutated); 9% (5/53) of patients with *IDH*-WT gliomas had initiated treatment prior to imaging, while 34% (13/38) patients with *IDH*-mutated tumors had initiated steroid use prior to imaging. Incorporating steroid use as a feature in our model did not significantly improve *IDH* prediction.

MRI Features and Univariate Analyses

From each patient's imaging, 2970 features were extracted. A total of 386 features remained after removing redundant features. The nonredundant features included 14 anatomical location, 27 shape, 114 texture, 212 parametric intensity, and 19 histogram features.

We also evaluated individual MRI features, which were previously associated with *IDH* status, for their predictive

Table 1 Patient characteristics

	Training (n = 90)	Validation (n = 30)	Total (n = 120)
Grade III (n; %)	26; 29%	9; 30%	35; 29%
Grade IV (n; %)	64; 71%	21; 70%	85; 71%
IDH-mutated (n; % column)	41; 46%	13; 43%	54; 45%
Age (years; mean; range)	51.4; 22–75	52.4; 20–85	51.65; 30–85
Sex (n male; % column)	52; 58%	16; 53%	68; 57%

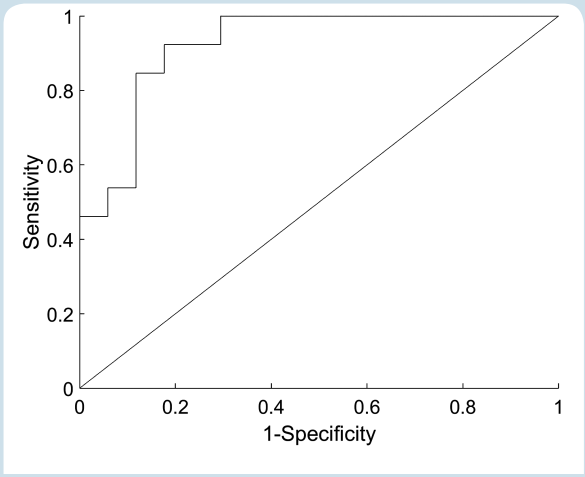

Fig. 2 Receiver operating characteristic (ROC) curve for *IDH* genotype prediction in validation cohort. Area under curve = 0.9231.

value in determining *IDH* genotype within our cohort.[12,13,36] The univariable AUCs for these MRI features tested on all 120 glioma were as follows (listed in order from least to most predictive): frontal or temporal tumor location (AUC = 0.5051), ADC (AUC = 0.5098), laterality (AUC = 0.5185), and T2/FLAIR volume (AUC = 0.6758).

Genotype Prediction

IDH genotype prediction using our model achieved accuracies of 86% (AUC = 0.8830) in the training cohort and 89% (AUC = 0.9231) in the validation cohort (Fig. 2). The mean predictive model scores for WT and mutant gliomas were 0.36 (95% confidence interval [CI], 0.30–0.41) and 0.59 (95% CI, 0.52–0.65), respectively ($P < .0001$) (Fig. 3). The training set classification error based on 10-fold cross validation was 0.1667. The 10 features that contributed most to our model are shown in Table 2. Patient age was the most important feature in our classifier; the relationship between age and *IDH* genotype is depicted in Fig. 3. To assess the impact of MRI features alone, we generated a model excluding age and sex; this model achieved prediction accuracies of 81% (AUC = 0.81) in the training cohort and 90% (AUC = 0.90) in the validation cohort with a training misclassification error of 0.1778.

Subgroup analyses revealed that the combined model with MRI and clinical features predicted *IDH* genotype of grade III and grade IV tumors with accuracies of 77.78% (AUC could not be calculated due to small sample size of grade III *IDH*-WT tumors) and 85.17% (AUC = 0.9265) in the validation cohort, respectively. The predictive model scores for WT and mutated gliomas separated by grade are shown in Fig. 4.

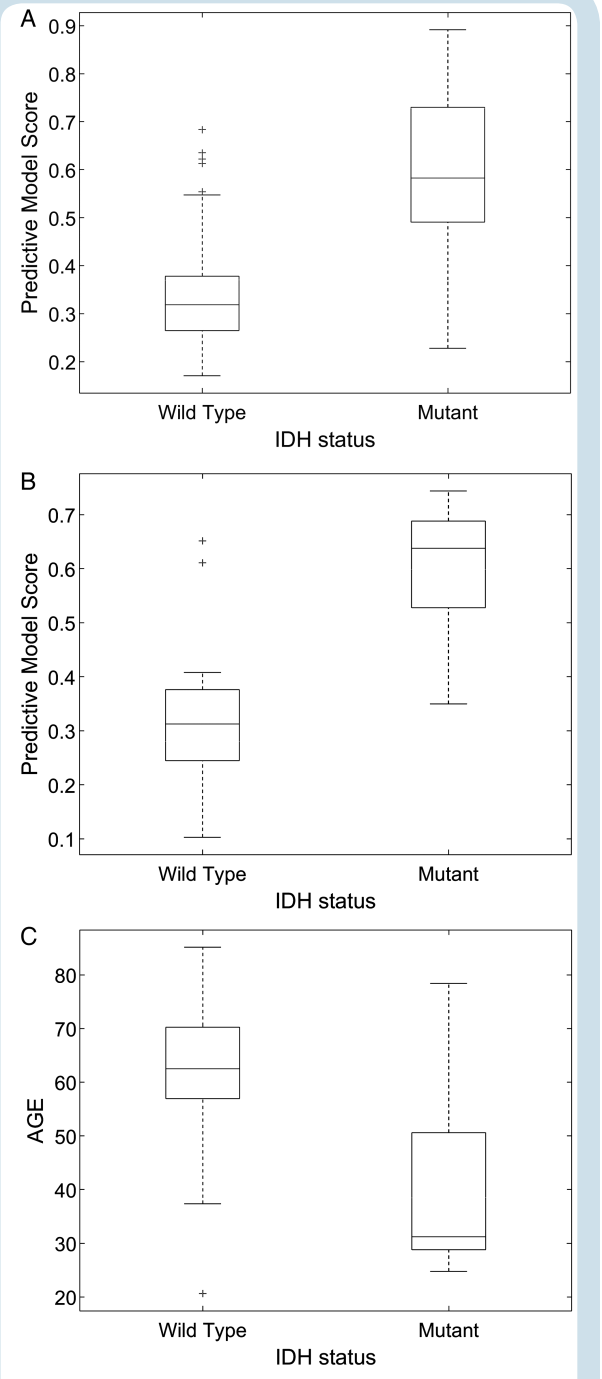

Fig. 3 Random forest classifier scores for *IDH*-wild-type and -mutated high-grade gliomas (HGGs) in the (A) training cohort and (B) validation cohort. Age (years) of patients with *IDH*-wild-type and -mutated HGGs in the validation cohort (C).

Discussion

In this study, a random forest classifier was created to integrate clinical data with multimodal, preoperative imaging features to predict *IDH* genotype in high-grade gliomas. Our model achieved 86% accuracy in the training cohort and 89% prediction accuracy in the validation cohort. This model only relied on patient age and imaging features extracted from a standard, preoperative MRI protocol including conventional T1, T2, and diffusion weighted imaging.

Table 2 Top-performing nonredundant features in univariate prediction of *IDH* genotype based on area under receiving operator characteristic curve in the validation cohort

Feature Type	Mask; Submask; Image	Feature	Training AUC	Validation AUC
Clinical	N/A	Patient age	0.8333	0.8552
Parametric	T1;T1; N/A	Enhancement intensity	0.6779	0.7104
Texture: co-occurrence	T1; ADC <1100 10^{-6} mm^2/s; ADC	Information measure of correlation[a], ×direction	0.7760	0.7738
Texture: co-occurrence	Nonenhancing tumor (T2/FLAIR); N/A; ADC	Information measure of correlation, ×direction	0.7651	0.7647
Texture: co-occurrence	T2 border; N/A; ADC	Information measure of correlation, ×direction	0.7511	0.7919
Texture: co-occurrence	T1 border; N/A; ADC	Information measure of correlation, ×direction	0.7466	0.6380
Texture: co-occurrence	Nonenhancing tumor (T2/FLAIR); ADC <1350 10^{-6} mm^2/s; N/A	Compactness[a]	0.7466	0.8642
Shape: volume	T1c:T2/FLAIR; N/A; N/A	Tumor volume-to-edema ratio	0.6750	0.7059
Parametric	T1; ADC <1350 10^{-6} mm^2/s; N/A	Enhancement intensity	0.7601	0.6968
Texture: co-occurrence	T2; ADC <1100 10^{-6} mm^2/s; ADC	Inverse correlation[a]	0.6934	0.7828

Abbreviations: ADC, apparent diffusion coefficient; AUC, area under the curve: FLAIR, fluid-attenuated inversion recovery.
[a]Information measure of correlation, compactness, and inverse correlation are texture features that have been previously applied to classify gliomas by degree of malignancy[54] and to predict survival outcomes in grade IV gliomas.[55]Detailed equations for these texture features are described elsewhere.[55,56]

Our analyses expand on the work of several recent studies that have uncovered novel associations among MRI features and glioma expression profiles. Macyszyn et al. created a model with a support vector machine classifier that utilized imaging features to separate WHO grade IV gliomas by expression profile (proneural, neural, mesenchymal, and classical)[18]; we utilized a different machine-learning technique (random forest) to build a model with clinical and imaging features to predict *IDH* genotype in a combined cohort of WHO grade III and IV gliomas. Previous groups have correlated qualitative MRI features with *IDH1* mutation in grade III and IV gliomas separately (specifically, Qi et al. and Sonoda et al. identified MRI features associated with grade III gliomas,[12,39] while Yashimata et al. evaluated features of grade IV gliomas.[40] To date, *IDH* prediction in a combined cohort of grades III and IV has not been attempted. Such a study may be of clinical importance given that *IDH* genotype may be a more useful prognostic marker than WHO grade; patients with *IDH*-WT grade III tumors have been shown to exhibit worse prognosis than those with *IDH*-mutated grade IV tumors.[6] Here, machine learning enabled the integration of clinical data with quantitative, multimodal imaging features to build a model predictive of *IDH* genotype in a combined grade III and IV glioma cohort.

The features that contributed most to *IDH* genotype prediction in our model included age and MRI parametric intensity, texture, and shape features. Not surprisingly, patient age was the most important feature in our model, reflecting the observation that patients with *IDH*-mutated glioma present at a significantly younger age than those with *IDH*-WT tumors.[41,42] Of note, one other clinical feature (ie, steroid use) yielded a significant finding: more patients with *IDH*-WT tumors than *IDH*-mutated tumors had initiated steroid treatment at the time of preoperative imaging. This difference has not been reported previously and could be explored on other datasets. While steroid treatment has been shown to affect the appearance of tumors by reducing contrast permeability and peritumoral edema,[20,37,38] including this feature in our model did not improve *IDH* prediction. The remaining top 10 features contributing to *IDH* prediction were MRI features, and 8 among them were obtained by filtering tumor volumes using ADC thresholds rather than the whole tumor volumes. The utility of DWI in glioma prognostication has been demonstrated previously[20,26,43,44]; we corroborated the utility of DWI to subselect volumes of interests with greater contribution to our model performance.

Several multimodal texture and parametric intensity features also contributed highly to our predictive model, although the underlying biological mechanism for how these features relate to *IDH* mutation is presently unclear. Past studies in glioma have correlated *IDH* genotype with intratumoral heterogeneity as well as with tumor margins based on qualitative assessment of conventional MRI.[12,13] Both texture and parametric intensity features extracted from MRI in our study may provide quantitative measures of such tissue heterogeneity within the tumor as well as along tumor margins. In addition, the textural features used in our model have been previously applied to distinguish gliomas based on *MGMT* promoter methylation status.[45,46] Brown et al. also found that texture features could be used to predict 1p/19q co-deletion in low-grade gliomas,[47] and Liu et al. observed associations between texture features and *p53* and *MIB-1* genotype.[48]

While we tested our combined features model in predicting *IDH* genotype, we also evaluated the predictive value of individual MRI features. No individual MRI feature achieved greater accuracy in predicting *IDH* genotype than the

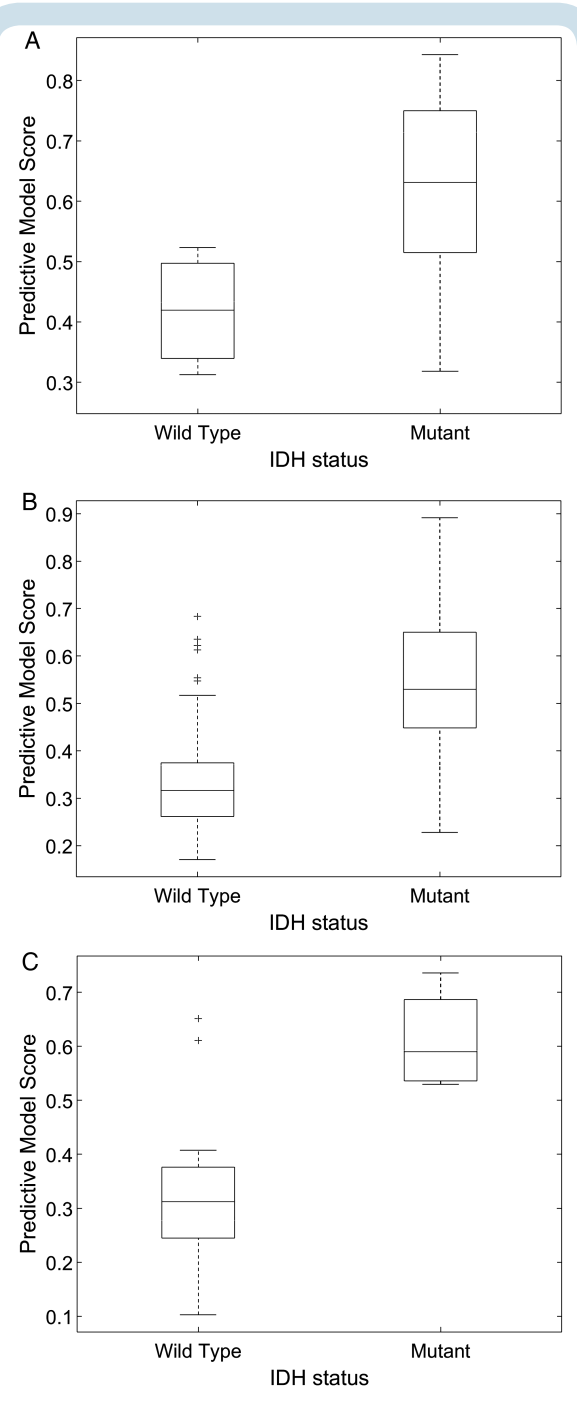

Fig. 4 Random forest classifier scores for *IDH*-wild-type and -mutated (A) WHO grade III gliomas in the training cohort, (B) WHO grade IV gliomas in the training cohort, and (C) WHO grade IV gliomas in the validation cohort. The area under the curve could not be calculated for WHO grade III tumors in the validation cohort due to small sample size.

combined model. This observation underscores the advantage of using a machine-learning algorithm to discover and integrate synergistic multimodal imaging features.

We also examined MRI features previously identified to vary with *IDH* genotype: frontoinsular-temporal tumor location, laterality, T2/FLAIR volume, and ADC.[12,13,36,39] Among these features, only T2/FLAIR volume (AUC = 0.6758) achieved an AUC >0.6. While T2/FLAIR volume was removed as a redundant feature in our pipeline, an associated feature (ie, contrast-enhancing tumor to T2/FLAIR volume) did contribute to our combined model. This finding concurs with previous studies that have broadly evaluated contrast enhancement and T2/FLAIR in *IDH*-mutated gliomas. Qi et al. correlated the extent of contrast enhancement with *IDH1* genotype in grade III gliomas,[12] while Carrillo et al. identified an association between the presence of noncontrast-enhancing tumor and *IDH1* mutation in grade IV gliomas.[49] MRI parameters combining contrast enhancement with nonenhancing perilesional FLAIR hyperintensity have also been reported to predict *IDH1* mutation in grade IV gliomas.[50] Recent studies have also suggested that MR spectroscopy is a promising noninvasive technique for identifying *IDH*-mutated gliomas through detection of intratumoral 2-HG.[51–53] Perfusion imaging features such as measures of tumor blood flow may also be of added value in *IDH* genotype prediction.[40] Our multimodality model may be improved by the addition of these imaging features in the future. Improvements in *IDH* prediction, however, would have to be balanced with the added complexity of obtaining MR spectroscopy and perfusion imaging (not currently part of standard imaging protocol) when optimizing for clinical utility. The features utilized in the current model are extracted from conventional MRI only.

There are several other important limitations to our study. Few *IDH*-WT grade III gliomas ($n = 3$) were included in these analyses due to strict eligibility requirements for both genetic and MRI data. All *IDH*-WT gliomas in our cohort had sequencing data to avoid inclusion of tumors with *IDH* mutations not detected by immunochemistry. Our model was also generated based on single-institution, retrospectively collected data, and its generalizability depends on feature stability that can be impacted by differences in imaging acquisition protocols as well as the reproducibility of image postprocessing and tumor segmentation. Our model needs, therefore, to be further validated using independent data. In addition, while a large number of imaging features have been incorporated into our model, our machine-learning approach did not provide the biological significance of individual features and how they interact with each other. Further work is needed to characterize and refine these features to potentially improve model performance. Finally, the processing time required to generate our model may also be a limitation to its clinical adoption, but hopefully this can be reduced with availability of validated, automated tumor segmentation algorithms.

The current study used machine-learning algorithms to generate a model that predicted *IDH* genotype in high-grade gliomas based on patient age as well as quantitative imaging features derived from standard, preoperative MRI. Our model achieved an accuracy of 89% in the validation cohort and may have the potential to serve as a noninvasive tool that provides important prognostic information and aids operative planning.

Supplementary Material

Supplementary material is available online at *Neuro-Oncology* (http://neuro-oncology.oxfordjournals.org/).

Conflict of interest statement. D.A.R. has the following conflicts of interest to disclose: (1) Advisory board – Abbvie, Amgen, BMS, Cavion, Celldex, EMD Serono, Genentech/Roche, Inovio, Juno Pharmaceuticals, Merck, Midatech, Momenta Pharmaceuticals, Novartis, Novocure, Oxigene, Regeneron, Stemline Therapeutics. (2) Lab Research Support – Celldex Therapeutics, Incyte, Midatech. (3) Speaker – Genentech/Roche, Merck, Novocure.

References

1 Ostrom QT, Gittleman H, Fulop J, et al. CBTRUS Statistical Report: Primary Brain and Central Nervous System Tumors Diagnosed in the United States in 2008–2012. *Neuro Oncol*. 2015;17(Suppl 4):iv1–iv62.
2 Parsons DW, Jones S, Zhang X, et al. An integrated genomic analysis of human glioblastoma multiforme. *Science*. 2008;321(5897):1807–1812.
3 Yan HPD, Jin G, McLendon R, et al. IDH1 and IDH2 mutations in gliomas. *N Engl J Med*. 2009;360(8):765–773.
4 Hartmann C, Meyer J, Balss J, et al. Type and frequency of IDH1 and IDH2 mutations are related to astrocytic and oligodendroglial differentiation and age: a study of 1,010 diffuse gliomas. *Acta Neuropathol*. 2009;118(4):469–474.
5 Houillier C, Wang X, Kaloshi G, et al. IDH1 or IDH2 mutations predict longer survival and response to temozolomide in low-grade gliomas. *Neurology*. 2010;75(17):1560–1566.
6 Hartmann C, Hentschel B, Wick W, et al. Patients with IDH1 wild type anaplastic astrocytomas exhibit worse prognosis than IDH1-mutated glioblastomas, and IDH1 mutation status accounts for the unfavorable prognostic effect of higher age: implications for classification of gliomas. *Acta Neuropathol*. 2010;120(6):707–718.
7 Flavahan WA, Drier Y, Liau BB, et al. Insulator dysfunction and oncogene activation in IDH mutant gliomas. *Nature*. 2016;529(7584):110–114.
8 Cryan JB, Haidar S, Ramkissoon LA, et al. Clinical multiplexed exome sequencing distinguishes adult oligodendroglial neoplasms from astrocytic and mixed lineage gliomas. *Oncotarget*. 2014;5(18):8083–8092.
9 Gutman DA, Dunn WDJr., Grossmann P, et al. Somatic mutations associated with MRI-derived volumetric features in glioblastoma. *Neuroradiology*. 2015;57(12):1227–1237.
10 Beiko J, Suki D, Hess KR, et al. IDH1 mutant malignant astrocytomas are more amenable to surgical resection and have a survival benefit associated with maximal surgical resection. *Neuro Oncol*. 2014;16(1):81–91.
11 Ellingson BM. Radiogenomics and imaging phenotypes in glioblastoma: novel observations and correlation with molecular characteristics. *Curr Neurol Neurosci Rep*. 2015;15(1):506.
12 Qi S, Yu L, Li H, et al. Isocitrate dehydrogenase mutation is associated with tumor location and magnetic resonance imaging characteristics in astrocytic neoplasms. *Oncol Lett*. 2014;7(6):1895–1902.
13 Metellus P, Coulibaly B, Colin C, et al. Absence of IDH mutation identifies a novel radiologic and molecular subtype of WHO grade II gliomas with dismal prognosis. *Acta Neuropathol*. 2010;120(6):719–729.
14 Tozer DJ, Jager HR, Danchaivijitr N, et al. Apparent diffusion coefficient histograms may predict low-grade glioma subtype. *NMR Biomed*. 2007;20(1):49–57.
15 Just N. Improving tumour heterogeneity MRI assessment with histograms. *Br J Cancer*. 2014;111(12):2205–2213.
16 Ellingson BM, Lai A, Harris RJ, et al. Probabilistic radiographic atlas of glioblastoma phenotypes. *AJNR Am J Neuroradiol*. 2013;34(3):533–540.
17 Emblem KE, Pinho MC, Zollner FG, et al. A generic support vector machine model for preoperative glioma survival associations. *Radiology*. 2015;275(1):228–234.
18 Macyszyn L, Akbari H, Pisapia JM, et al. Imaging patterns predict patient survival and molecular subtype in glioblastoma via machine learning techniques. *Neuro Oncol*. 2015;18(3):417–425.
19 Zacharaki EI, Morita N, Bhatt P, O'Rourke DM, Melhem ER, Davatzikos C. Survival analysis of patients with high-grade gliomas based on data mining of imaging variables. *AJNR Am J Neuroradiol*. 2012;33(6):1065–1071.
20 Ellingson BM, Malkin MG, Rand SD, et al. Volumetric analysis of functional diffusion maps is a predictive imaging biomarker for cytotoxic and anti-angiogenic treatments in malignant gliomas. *J Neurooncol*. 2011;102(1):95–103.
21 Fuller GN, Scheithauer BW. The 2007 Revised World Health Organization (WHO) Classification of Tumours of the Central Nervous System: newly codified entities. *Brain Pathol*. 2007;17(3):304–307.
22 Ramkissoon SH, Bi WL, Schumacher SE, et al. Clinical implementation of integrated whole-genome copy number and mutation profiling for glioblastoma. *Neuro Oncol*. 2015;17(10):1344–1355.
23 Thomas RK, Baker AC, Debiasi RM, et al. High-throughput oncogene mutation profiling in human cancer. *Nat Genet*. 2007;39(3):347–351.
24 Wagle N, Berger MF, Davis MJ, et al. High-throughput detection of actionable genomic alterations in clinical tumor samples by targeted, massively parallel sequencing. *Cancer Discov*. 2012;2(1):82–93.
25 Murphy SN, Herrick C, Wang Y, et al. High throughput tools to access images from clinical archives for research. *J Digit Imaging*. 2015;28(2):194–204.
26 Huang RY, Rahman R, Hamdan A, et al. Recurrent glioblastoma: volumetric assessment and stratification of patient survival with early posttreatment magnetic resonance imaging in patients treated with bevacizumab. *Cancer*. 2013;119(19):3479–3488.
27 Pieper S, Lorensen B, Schroeder W, Kikinis R. The NA-MIC Kit: ITK, VTK, pipelines, grids and 3D slicer as an open platform for the medical image computing community. Proceedings of the 3rd IEEE International Symposium on Biomedical Imaging: Macro to Nano. 2006;698–701.
28 Pieper S, Halle M, Kikinis R. 3D SLICER. Proc. 1st IEEE Int. Symp. Biomed. Imaging Nano Macro. 2004;632–635.
29 Breiman L. Random forests. *Mach Learn*. 2001;45:5–32.
30 Chang JS, Yeh RF, Wiencke JK, et al. Pathway analysis of single-nucleotide polymorphisms potentially associated with glioblastoma multiforme susceptibility using random forests. *Cancer Epidemiol Biomarkers Prev*. 2008;17(6):1368–1373.
31 Ranjith G, Parvathy R, Vikas V, Chandrasekharan K, Nair S. Machine learning methods for the classification of gliomas: Initial results using features extracted from MR spectroscopy. *Neuroradiol J*. 2015;28(2):106–111.
32 Oshiro TM, Perez PD, Baanauskas J. Semi Supervised Clustering: A Pareto Approach. *Mach Learn Data Min Pattern Recognit*. 2012;7376(January):237–251.
33 MathWorks. *OOBPermutedVarDeltaError property*, 2016. Available at http://www.mathworks.com/help/stats/treebagger.oobpermutedvardeltaerror.html (accessed 24 May 2016).
34 Dang L, Jin S, Su SM. IDH mutations in glioma and acute myeloid leukemia. *Trends Mol Med*. 2010;16(9):387–397.
35 Yen KE, Bittinger MA, Su SM, Fantin VR. Cancer-associated IDH mutations: biomarker and therapeutic opportunities. *Oncogene*. 2010;29(49):6409–6417.
36 Lee S, Choi SH, Ryoo I, et al. Evaluation of the microenvironmental heterogeneity in high-grade gliomas with IDH1/2 gene mutation using histogram analysis of diffusion-weighted imaging and dynamic-susceptibility contrast perfusion imaging. *J Neurooncol*. 2015;121(1):141–150.
37 Zaki HS, Jenkinson MD, Du Plessis DG, Smith T, Rainov NG. Vanishing contrast enhancement in malignant glioma after corticosteroid treatment. *Acta Neurochir (Wien)*. 2004;146(8):841–845.

38 Andersen C, Astrup J, Gyldensted C. Quantitation of peritumoural oedema and the effect of steroids using NMR-relaxation time imaging and blood-brain barrier analysis. *Acta Neurochir Suppl (Wien).* 1994;60:413–415.

39 Sonoda Y, Shibahara I, Kawaguchi T, et al. Association between molecular alterations and tumor location and MRI characteristics in anaplastic gliomas. *Brain Tumor Pathol.* 2015;32(2):99–104.

40 Yamashita K, Hiwatashi A, Togao O, et al. MR Imaging-Based Analysis of Glioblastoma Multiforme: Estimation of IDH1 Mutation Status. *AJNR Am J Neuroradiol.* 2016;37(1):58–65.

41 Paugh BS, Qu C, Jones C, et al. Integrated molecular genetic profiling of pediatric high-grade gliomas reveals key differences with the adult disease. *J Clin Oncol.* 2010;28(18):3061–3068.

42 Pollack IF, Hamilton RL, Sobol RW, et al. IDH1 mutations are common in malignant gliomas arising in adolescents: a report from the Children's Oncology Group. *Childs Nerv Syst.* 2011;27(1):87–94.

43 Saraswathy S, Crawford FW, Lamborn KR, et al. Evaluation of MR markers that predict survival in patients with newly diagnosed GBM prior to adjuvant therapy. *J Neurooncol.* 2009;91(1):69–81.

44 Crawford FW, Khayal IS, McGue C, et al. Relationship of pre-surgery metabolic and physiological MR imaging parameters to survival for patients with untreated GBM. *J Neurooncol.* 2009;91(3):337–351.

45 Drabycz S, Roldan G, de Robles P, et al. An analysis of image texture, tumor location, and MGMT promoter methylation in glioblastoma using magnetic resonance imaging. *Neuroimage.* 2010;49(2):1398–1405.

46 Levner I, Drabycz S, Roldan G, De Robles P, Cairncross JG, Mitchell R. Predicting MGMT methylation status of glioblastomas from MRI texture. *Med Image Comput Comput Assist Interv.* 2009;12(Pt 2):522–530.

47 Brown R, Zlatescu M, Sijben A, et al. The use of magnetic resonance imaging to noninvasively detect genetic signatures in oligodendroglioma. *Clin Cancer Res.* 2008;14(8):2357–2362.

48 Liu C, Zhang H, Pan Y, Huang F, Xia S. Towards MIB-1 and p53 detection in glioma magnetic resonance image: a novel computational image analysis method. *Phys Med Biol.* 2012;57(24):8393–8404.

49 Carrillo JA, Lai A, Nghiemphu PL, et al. Relationship between tumor enhancement, edema, IDH1 mutational status, MGMT promoter methylation, and survival in glioblastoma. *AJNR Am J Neuroradiol.* 2012;33(7):1349–1355.

50 Colen R, Ashour O, Zinn PO. Imaging genomic IDH-1 biomarker signature. *Neuro Oncol.* 2013;15(Suppl 3):iii191–iii205.

51 Pope WB, Prins RM, Albert Thomas M, et al. Non-invasive detection of 2-hydroxyglutarate and other metabolites in IDH1 mutant glioma patients using magnetic resonance spectroscopy. *J Neurooncol.* 2012;107(1):197–205.

52 Andronesi OC, Kim GS, Gerstner E, et al. Detection of 2-hydroxyglutarate in IDH-mutated glioma patients by in vivo spectral-editing and 2D correlation magnetic resonance spectroscopy. *Sci Transl Med.* 2012;4(116):116ra114.

53 Choi C, Ganji SK, DeBerardinis RJ, et al. 2-hydroxyglutarate detection by magnetic resonance spectroscopy in IDH-mutated patients with gliomas. *Nat Med.* 2012;18(4):624–629.

54 Zacharaki EI, Wang S, Chawla S, et al. Classification of brain tumor type and grade using MRI texture and shape in a machine learning scheme. *Magn Reson Med.* 2009;62(6):1609–1618.

55 Lee J, Jain R, Khalil K, et al. Texture feature ratios from relative CBV maps of perfusion MRI are associated with patient survival in glioblastoma. *AJNR Am J Neuroradiol.* 2016;37(1):37–43.

56 Haralick RM, Shanmugam K, Dinstein I. Textural features for image classification. *IEEE Trans Syst Man Cybern* 1973;3(6):610–621.